

X-NeMo: EXPRESSIVE NEURAL MOTION REENACTMENT VIA DISENTANGLED LATENT ATTENTION

Anonymous authors

Paper under double-blind review

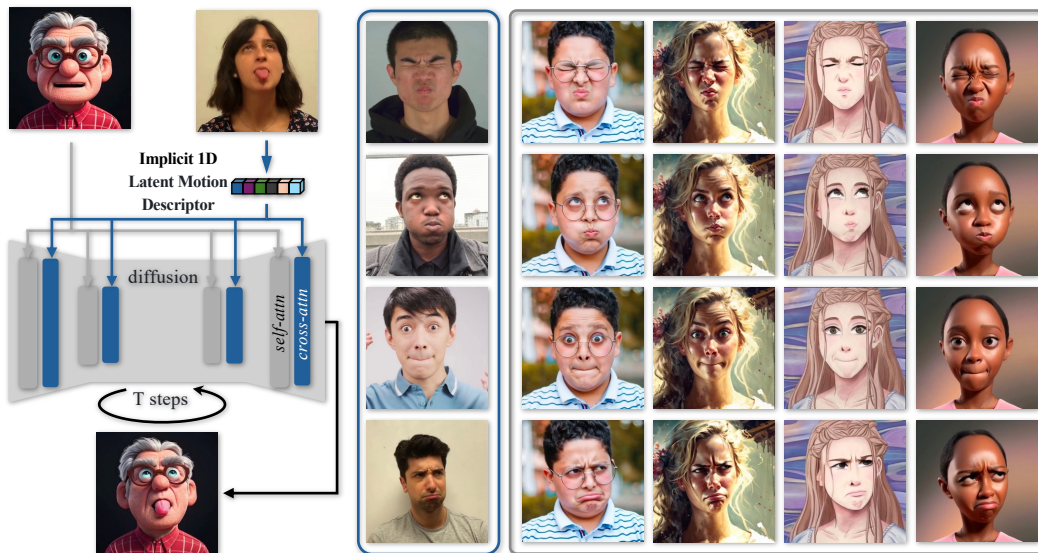


Figure 1: We present X-NeMo, a diffusion-based portrait animation framework that integrates expressive 1D latent motion descriptors with identity-disentangled motion control through cross-attention mechanisms (left). Our method enables meticulous transfer of expressive head poses and detailed facial expressions while maintaining identity consistency, even across subjects with distinct appearances, styles and facial structures (right).

ABSTRACT

We propose X-NeMo, a novel zero-shot diffusion-based portrait animation pipeline that animates a static portrait using facial movements from a driving video of a different individual. Our work first identifies the root causes of the key issues in prior approaches, such as identity leakage and difficulty in capturing subtle and extreme expressions. To address these challenges, we introduce a **self-supervised** training framework that distills a 1D identity-agnostic latent motion descriptor from driving image, effectively controlling motion through cross-attention during image generation. Our implicit motion descriptor captures expressive facial motion in fine detail, learned from a diverse video dataset without reliance on pretrained motion detectors. We further enhance expressiveness and disentangle motion latents from identity cues by supervising their learning with a dual GAN decoder, alongside spatial and color augmentations. By embedding the driving motion into a 1D latent vector and controlling motion via cross-attention rather than additive spatial guidance, our design eliminates the transmission of spatial-aligned structural clues from the driving condition to the diffusion backbone, substantially mitigating identity leakage. Extensive experiments demonstrate that X-NeMo surpasses state-of-the-art baselines, producing highly expressive animations with superior identity resemblance. Our code and models will be available for research.

1 INTRODUCTION

We investigate the task of portrait animation, where a static portrait is animated using head movements and facial expressions derived from a driving video of a different subject. This task has garnered growing interest owing to its versatile applications in video conferencing, visual effects and digital agents. Building on prior research, we aim to advent the field of zero-shot portrait reenactment by synthesizing *highly expressive* animations while maintaining *identity resemblance* to the reference portraits with minimal loss.

Commencing with the pioneering works Siarohin et al. (2019b;a), portrait animation has primarily involved extracting motion features from a driving video followed with a generative process, such as GANs Goodfellow et al. (2014); Karras et al. (2019; 2020) or diffusion models Ho et al. (2020); Song et al. (2020a;b); Rombach et al. (2022), conditioned on the reference appearance and derived motion features. Recent advancements in diffusion models have achieved unprecedented diversity and quality in image generation, prompting us to utilize their generative capabilities Saharia et al. (2022); AI (2022) for portrait animation. Recent approaches have tackled portrait animation as a controlled image-to-video diffusion task, where the reference appearance is cross-queried through mutual self-attention Cao et al. (2023) whereas the driving motion signal is integrated into the denoising process using frameworks like ControlNet Zhang et al. (2023b) or lighter-weight PoseGuider Hu et al. (2023). The driving motion is represented either through explicit semantic signals such as facial landmarks Ma et al. (2024); Wei et al. (2024); Chang et al. (2024), dense pose Xu et al. (2024d) and facial template renderings Chen et al. (2024a), or through implicit motion features learnt from synthetic cross-identity image pairs with aligned expression but different identities Xie et al. (2024); Yang et al. (2024a). Despite significant progress in realism and dynamics, these diffusion-based methods still struggle to capture extreme or subtle expressions and often suffer from identity drifting, particularly when the reference and driving identities differ substantially.

We identify two main factors contributing to the challenges in expressiveness and identity resemblance in prior network designs. First, explicit motion descriptors like facial landmarks or blend-shapes, are often too coarse to capture extreme or subtle facial motions and rely heavily on the robustness and accuracy of external motion detectors. Although these descriptors do not contain RGB appearance, they encode the facial structure of the driving identity, leading to undesirable identity leakage in cross-identity animations. Recent approaches Xie et al. (2024); Yang et al. (2024a) have attempted to derive implicit motion signals directly from synthetic cross-identity training image pairs generated using an off-the-shelf portrait animator (e.g., Wang et al. (2021)). Despite substantial improvements in expressiveness and stability, these methods remain constrained by the capacity of pre-trained portrait animators which struggle with complex expressions (e.g., tongue protrusion, cheek puffing). Additionally, sharing aligned facial structures in training pairs inadvertently pass identity information onto the learnt implicit motion features. Second, prior diffusion-based approaches often guide motion control using spatially-aligned 2D conditions via ControlNet or PoseGuider. While effective for self-driven motion, this approach encourages the diffusion backbone to take a shortcut to mimic the 2D layout rather than fully leveraging semantic mappings between reference and driving images, leading to identity leakage during expression transfer across different subjects.

In this work, we propose X-NeMo, a novel portrait animation framework that enables self-supervised learning of a compact 1D latent motion descriptor, facilitating effective motion control in diffusion models via *cross attentions*. Specifically, we introduce a motion encoder to extract a 1-D *identity-agnostic* motion latent from the original driving image, and modulate this controlling motion descriptor into the diffusion backbone via cross-attentions. By training *jointly* with the image generator, our encoder fully leverages the motion diversity and richness embedded in our training video collections, without reliance on off-the-shelf motion detectors. We restrict the dimensionality of the latent embedding, functioning as a low-pass filter Burkov et al. (2020), and format it as a 1D global motion descriptor that excludes 2D structural cues from the driving image. Furthermore, by using cross motion attentions rather than spatial additive guidance, we ensure that the backbone remains agnostic to the identity structural signals from the motion control branch. This structure-agnostic motion control enables various augmentations like color jittering and spatial transformations, promoting the self-supervised disentanglement of identity and motion. In addition to the diffusion loss, we incorporate a dual GAN-based decoder head and refine the learning of our motion latent space with image-level losses that capture subtle and detailed expressions. Our design effectively mitigates the aforementioned shortcut learning, and compels the network to interpret fine-grained motion semantics during both motion encoding and image generation stages.

Trained on a collective of public video datasets Zhang et al. (2021); Xie et al. (2022); Kirschstein et al. (2023), our method excels at faithfully capturing both extreme and nuanced facial motions and transferring them across subjects even with distinct identity attributes. We extensively evaluate our model across our challenging benchmarks and X-NeMo outperforms state-of-the-art portrait animation baselines both quantitatively and qualitatively. Additionally, our expressive latent motion descriptor serves as a unified identity-agnostic embedding, facilitating motion interpolation and video outpainting applications beyond portrait animation. We summarize our contributions as follows,

- A novel diffusion-based portrait animation pipeline, **coupled with latent motion representation**, achieving state-of-the-art performance in terms of motion accuracy and identity disentanglement.
- A structure-agnostic motion control scheme that learns a 1-D identity-disentangled latent motion descriptor and modulates control into image generation via cross-attentions, effectively addressing the long-standing issues of identity entanglement and motion expressiveness loss.
- A set of carefully designed strategies during both training (e.g., dual head latent supervision, augmentations and reference feature masking) and inference that substantially enhance the model performance, as supported by extensive ablation studies.
- Demonstration of captivating zero-shot portrait animations and generations.

2 RELATED WORKS

GAN-based Portrait Animation. Video-driven face reenactment seeks to accurately transfer facial expressions and head movements from a driving video to a target image. Common approaches have primarily leveraged Generative Adversarial Networks (GANs) Goodfellow et al. (2014); Karas et al. (2019; 2020) to model and capture the intricate motion dynamics between source and target identities. Broadly, these methods can be categorized into two classes: The first class is based on *explicit motion representations* Siarohin et al. (2019a;b); Ren et al. (2021); Wang et al. (2021); Mallya et al. (2022); Yin et al. (2022); Gao et al. (2023); Doukas et al. (2021); Guo et al. (2024a); Zhao & Zhang (2022), such as 3D face model parameters, landmarks, or latent keypoints, which use structured information to disentangle appearance and motion, but struggle with large pose changes or dynamic expressions. The second category involves *latent motion representations* Burkov et al. (2020); Liang et al. (2022); Zhou et al. (2021); Pang et al. (2023); Wang et al. (2022; 2023); Drobyshev et al. (2022; 2024); Xu et al. (2024c), embedding motion information in a latent space, offering improved expressiveness but relying on complex loss functions and hyperparameters to achieve identity-motion disentanglement. While more effective at transferring subtle expressions, such methods are still limited by the capability of GAN-based generators in handling extreme expressions and out-of-domain portrait styles. Our work follows this disentangled representation learning approach, but instead we use a Diffusion Model as the generator, which offers significantly improved generation capabilities with diverse and complex portrait styles.

Diffusion-based Portrait Animation. Diffusion models Ho et al. (2020); Song et al. (2020a;b) have demonstrated strong generative capabilities, with Latent Diffusion Models (LDMs) Rombach et al. (2022) further advancing its efficiency by operating in a lower-dimensional latent space. Recent works Liu et al. (2024); Xu et al. (2024a); Han et al. (2023); Varanka et al. (2024); Paskaleva et al. (2024) have explored adapting pre-trained LDMs AI (2022) for conditional portrait generation, by mapping reference images and driving signals into the text embeddings (e.g., using CLIP Khandelwal et al. (2022)) and injecting them into cross-attention layers. While effective for coarse-level facial expression editing, these methods still struggle with appearance and motion consistency in portrait video animation. Hu et al. (2023); Xu et al. (2024d); Chang et al. (2024) designed for human body animation have shown that the combination of a dual U-Net with mutual self-attention Cao et al. (2023) and temporal module Guo et al. (2024b) is able to maintain motion smoothness with consistent appearance. This framework has been extended to portrait animation in several works Tian et al. (2024); Xie et al. (2024); Wei et al. (2024); Xu et al. (2024b); Yang et al. (2024a); Wang et al. (2024); Ma et al. (2024); Chen et al. (2024b), often using ControlNet Zhang et al. (2023b) or PoseGuider Hu et al. (2023) for motion control. During training, they rely on explicit representations like facial keypoints Ma et al. (2024); Wei et al. (2024), facial mesh renderings Chen et al. (2024a), or synthetic cross-identity portraits Xie et al. (2024); Yang et al. (2024a). In contrast, our method learns a latent motion representation **jointly** with our diffusion backbone, and incorporates motion control with cross-attentions, effectively preventing identity leakage.

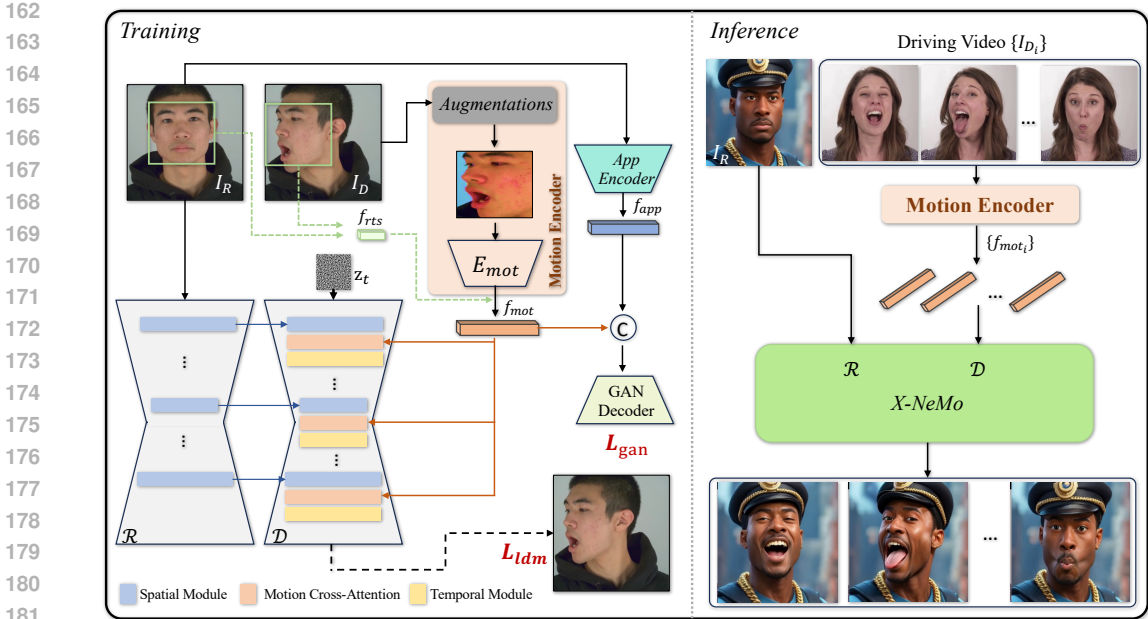


Figure 2: Overview of X-NeMo. We leverage a pretrained diffusion model \mathcal{D} as the rendering backbone and incorporate a reference network module \mathcal{R} for appearance conditioning, along with temporal modules for cross-frame consistency. For motion control, we train a latent motion embedding f_{mot} encoded from the driving image I_D after applying spatial and color augmentations. Alongside the relative translation and scaling f_{rts} of the face bounding box from reference I_R and driving image I_D , we integrate the latent motion conditions into the diffusion backbone using newly inserted cross-attention layers. Besides the original diffusion loss L_{ldm} , we supervise the learning of our latent motion embedding with a jointly trained GAN decoder head using image-level losses L_{gan} . During inference, we derive the latent motion codes directly from each driving frame, allowing us to synthesize expressive and precise animations while strictly maintain identity resemblance to the reference image.

3 METHOD

Given a single portrait as the reference image I_R , our objective is to generate a head animation sequence $\{I_{R \rightarrow D_i}\}$ of length l , conditioned on a driving video I_{D_i} , where $i = 1, \dots, l$ denotes the frame index. The generated frames $\{I_{R \rightarrow D_i}\}$ aim to preserve the identity features and background content depicted in I_R while accurately replicating the head pose and facial expressions featured in each corresponding driving frame I_{D_i} . While portrait animation algorithms are generally trained as a frame reconstruction task over video datasets, the I_R and I_D may feature distinct identities during inference, enabling cross-identity motion transfer.

For our task, we harness the generative capabilities of pre-trained Latent Diffusion Models AI (2022) for image generation. Although our method shares some network modules with prior diffusion-based approaches (Section 3.1), it innovates on motion control by addressing the root causes behind the loss of expressiveness and identity resemblance. We introduce our learning framework that achieves fine-grained, identity-agnostic motion control through cross-attention to a co-learned implicit motion descriptor (Section 3.2). To assist the self-supervised learning of motion and identity disentanglement, we present a set of carefully designed training strategies (Section 3.3). Figure 2 provides an overview of our training and inference pipeline.

3.1 PRELIMINARIES

Latent Diffusion Model. Facilitated by a pretrained auto-encoder, latent diffusion models Rombach et al. (2022) are a class of diffusion models Ho et al. (2020); Song et al. (2020a;b) that synthesize desired samples in the image latent space, starting from Gaussian noise $z_T \sim N(0, 1)$ and refining through T denoising steps. During training, latent representations of images are progressively

216 corrupted by Gaussian noise ϵ , following the Denoising Diffusion Probabilistic Model (DDPM)
 217 framework Ho et al. (2020). A UNet-based denoising backbone network \mathcal{D} containing intervened
 218 layers of convolutions and self-/cross-attentions, is trained to learn the reverse denoising process.

219 **Portrait Animation.** Recently a line of work Tian et al. (2024); Xie et al. (2024); Wei et al. (2024);
 220 Xu et al. (2024b); Yang et al. (2024a); Wang et al. (2024); Ma et al. (2024); Chen et al. (2024b)
 221 have explored leveraging the generative power of pretrained LDM, such as Stable Diffusion AI
 222 (2022), for portrait animation. While exhibiting slight algorithmic variations, these methods gener-
 223 ally employ similar components to transfer driving motions onto the reference image. Specifically,
 224 a reference network \mathcal{R} Cao et al. (2023), sharing the same architecture with the UNet \mathcal{D} , extracts
 225 reference features of identity appearance and background which are then cross-queried by the UNet
 226 self-attention blocks. Motion control is achieved through an additional module, often formatted in
 227 ControlNet Zhang et al. (2023b) or lighter-weight PoseGuider Hu et al. (2023), translating driving
 228 conditions into 2D spatially-aligned offsets additive to the UNet features. To maintain consistency
 229 across animated frames, temporal modules Guo et al. (2023), which incorporates cross-frame atten-
 230 tions, are intervened with the spatial transformer blocks.

231 While effective to some extent, prior methods often fall short in expressiveness and suffer from
 232 identity leakage in the generated animations. First, expressiveness is limited by the coarse granu-
 233 larity of the driving motion conditions, such as facial landmarks or synthetic training images Xie
 234 et al. (2024), which fail to capture complex and subtle expressions like frowning or puckering. Sec-
 235 ond, while prior approaches mostly address appearance leakage, they overlook the leakage of 2D
 236 facial structure and spatial layout embedded in the driving conditions, whether through landmarks or
 237 synthesized images. ControlNet-like mechanisms transform these motion conditions into spatially-
 238 aligned offsets within the UNet’s intermediate features. This reliance on spatial alignment causes the
 239 UNet to bypass the need to interpret semantic correspondences between the reference and driving
 240 faces, resulting in undesirable identity drift during cross-identity animation at inference.

241 3.2 PIPELINE WITH IDENTITY-DISENTANGLED IMPLICIT MOTION CONTROL

242
 243 As shown in Figure 2, we follow the existing UNet-based latent diffusion framework AI (2022),
 244 integrating both the reference network and temporal modules. However, our key innovation lies in
 245 a novel motion control module, designed to tackle challenges in motion expressiveness and identity
 246 consistency, particularly during cross-identity reenactments. A core design principle of our approach
 247 is to distill motion directly from the original driving images, while ensuring the image generation
 248 backbone operates independently of any appearance or structural clues from the motion control path.

249 **Latent Motion Descriptor.** For motion extraction, we employ an image encoder E_{mot} , to learn an
 250 implicit latent representation, f_{mot} , that captures facial motions across varying levels of granularity.
 251 Similar to the approaches in Wang et al. (2022; 2023), we formulate the motion latent representation
 252 f_{mot} as a *low-dimensional 1-D global* descriptor. The motion encoder E_{mot} consists of intervened
 253 layers of convolution-based feature extraction and self-attention, followed by MLP layers, which
 254 encode the motion into a 1D latent vector, thereby eliminating spatial positional information (i.e.,
 255 image structure) along the encoding process. Following the information bottleneck principle Tishby
 256 et al. (2000), we employ a larger network capacity (i.e., the reference net \mathcal{R}) and higher feature
 257 dimensions (i.e., multi-scale feature maps) for appearance modeling, while using a smaller network
 258 capacity (E_{mot}) and lower feature dimension (f_{mot}) for motion encoding. This design, function-
 259 ing as a low-pass bottleneck filter, encourages the emergence of disentangled representations that
 260 effectively capture key semantics of facial motion without entangling with appearance information.
 261 Furthermore, unlike previous methods that rely on pretrained motion extractor as the driving condi-
 262 tions (e.g., facial landmarks), our latent motion representation is [optimized jointly with the diffusion](#)
 263 [generator during training](#). As a result, this allows our model to progressively learn and refine the
 264 motion distribution as the diffusion model is trained on more diverse and expressive video data like
 265 NerSemble Kirschstein et al. (2023). With that, our approach enhances the expressiveness of the
 generated animations, as the model adapts to more complex and nuanced facial motions.

266 **Cross-Attention Control.** To exert motion control on UNet using our latent motion descriptor, one
 267 possible approach would be to use a ControlNet-like module to guide the denoising process after
 268 transforming the 1D latent code f_{mot} into a 2D spatially-aligned control map via a StyleGAN-like
 269 decoder. However, this would contradict our design goal for identity disentanglement.(Figure 3(a))
 Since f_{mot} is intentionally free of 2D structural information, transforming it into a spatial control

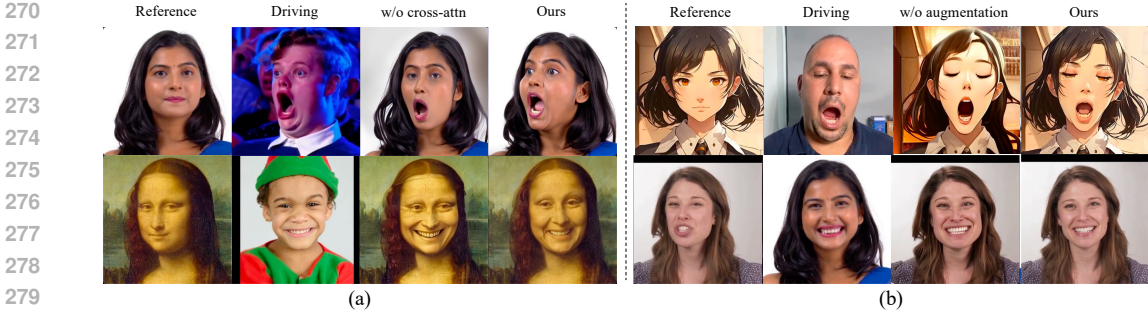


Figure 3: Qualitative ablation study on factors affecting identity consistency. (a) Replacing our motion cross-attentions with a control module using spatially additive guidance leads to severe leakage of the driving identity’s facial structure. (b) Training without our color and spatial augmentations results in noticeable appearance leakage and identity drift.

map demands additional input regarding the reference identity’s structure, thereby violating our principle that the motion control path should remain agnostic to identity-specific features. Instead the UNet should resort to the reference net for relevant identity-related information.

Instead, we adopt a cross-attention conditioning mechanism, which has proven effective across various control modalities Rombach et al. (2022); Tian et al. (2024); Ruiz et al. (2023). This allows direct injection of the latent motion embedding into the UNet without adding spatial bias. Specifically, we insert motion-attention layers performing cross attention with the latent motion code f_{mot} after each spatial transformer blocks in the backbone. This cross-attention scheme integrates the 1D motion embedding globally into the generation process, encouraging the UNet to interpret the motion condition and establish semantic correspondences between the reference and driving identity.

3.3 TRAINING STRATEGIES

For training, we randomly sample two distinct frames from a video as the reference I_R and driving I_D image, respectively. The model is then trained to denoise the latent map of the target image I_D at timestep t , with the diffusion loss defined as follows,

$$L_{ldm} = \mathbb{E}_{z_t, \epsilon \sim \mathcal{N}(0,1), t} [\|\epsilon - \epsilon_\theta(z_t, c_{ref}, f_{mot})\|_2^2], \tag{1}$$

where ϵ_θ denotes the trainable parameters in the backbone \mathcal{D} , and f_{mot}, c_{ref} represent the driving motion and reference features, respectively, extracted by E_{mot} and \mathcal{R} . The training process is structured into three stages. The first stage is the image pretraining stage, where the backbone UNet and reference net are taken into training. The second stage additionally incorporates the motion encoder E_{mot} and the newly integrated motion-attention layers into the optimization, forming an end-to-end encoder-generator structure. Lastly, we train the temporal modules to ensure cross-frame coherence. After the three-stage training process (intended as warm-up), we finetune the entire pipeline end-to-end, with all trainable modules optimized simultaneously.

However, straightforward self-supervised training of the entire framework does not inherently disentangle identity from facial motion. The UNet may inadvertently reconstruct the target image by borrowing appearance features from the driving image or encoding identity information into the latent motion descriptor f_{mot} . Additionally, when I_R and I_D share similar expressions, the model may distill motion signals from the reference image, hindering independent control over facial motion and identity, particularly in cross-identity reenactments. To address these issues, we propose several training strategies to fully leverage the potential of our network design in Section 3.2.

Color/Spatial Augmentation. To suppress identity information leakage from the motion control branch, we reduce the appearance and structural consistency between the driving and target images using both color and spatial augmentations. Specifically, we apply color jittering, random scaling within 30%, and piecewise affine transformations, to the driving image I_D , altering the facial appearance and shape while preserving motion semantics. We also perform face-centered cropping to enhance spatial disparity between the driving and target, promoting the motion encoder E_{mot} to focus on the facial movements and capture nuanced expressions. As shown in Figure 3(b), these augmentations effectively guide the motion encoder E_{mot} towards learning identity-agnostic mo-

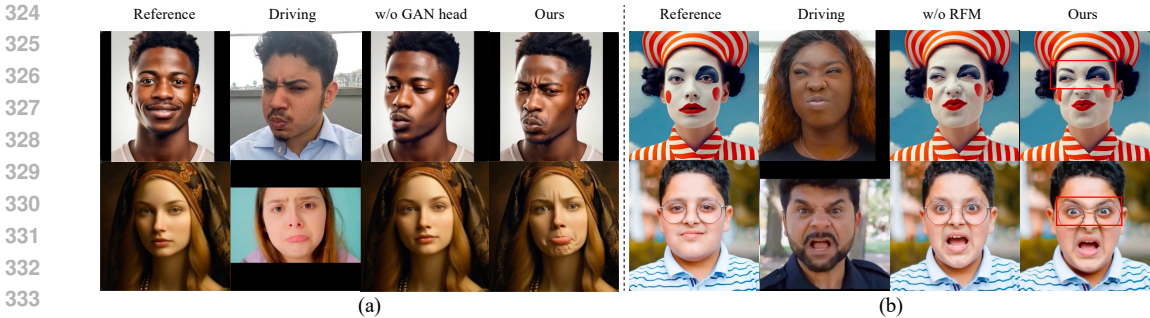


Figure 4: Qualitative ablation study on factors influencing motion expressiveness.(a) Without the dual GAN head, training solely with the diffusion loss hinders the motion encoder’s ability to learn detailed and local motion patterns. (b) Our reference feature masking (RFM) strategy facilitates the transfer of fine-level facial expressions, such as the wrinkles at the nasal region.

tion representation. To account for the disrupted head translation due to face-centered cropping, we construct a triplet $f_{rts} = (\Delta x/s_r, \Delta y/s_r, s_d/s_r)$, where $(\Delta x, \Delta y)$ denotes the 2D relative distance between the face centers in the I_R and I_D , and s_d/s_r reflects the change in bounding box scale. This triplet is processed through fully connected layers and fused with latent motion embedding f_{mot} .

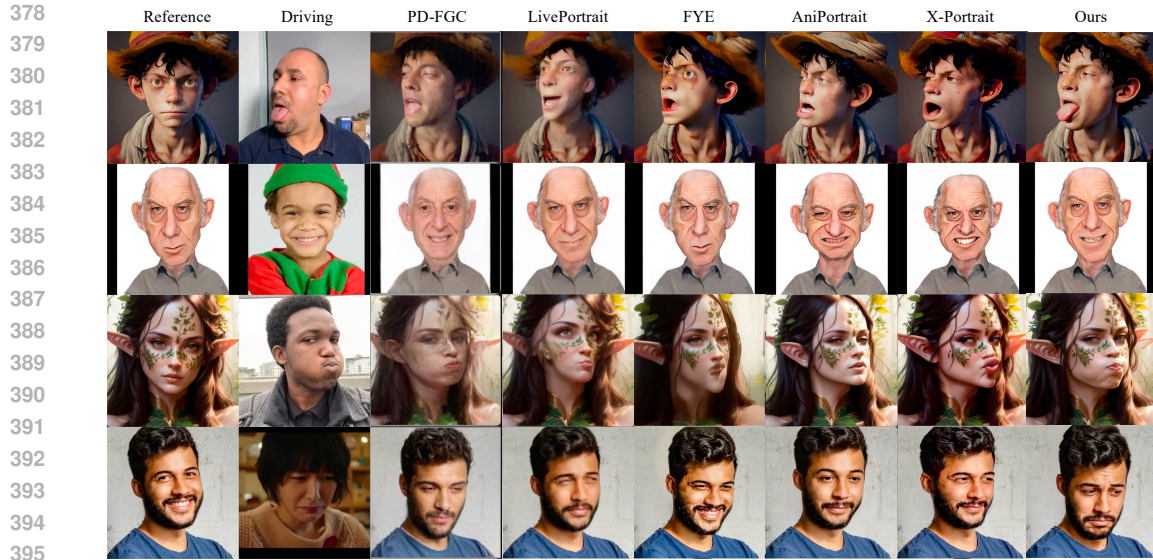
Owing to our design of motion control via latent motion embedding and cross-attentions, we substantially improves facial motion disentanglement from identity structure through spatial augmentations. In contrast, applying these augmentations with a ControlNet-like mechanism, which relies heavily on aligned spatial control signals, would degrade both robustness and accuracy.

Dual-Head Latent Supervision. In our early experiments, we observe that our motion control training, while effective in capturing coarse facial motions, converges slowly and struggles to depict subtle and fine-grained motions like frowning and puckering (see Figure 4(a)). The latent motion embedding, acting as a low-pass filter, tends to model low-frequency movements first. Additionally, the diffusion loss used during training assigns equal weight to every “pixel” in the latent noise, leading the model to prioritize a smooth motion space over capturing local, detailed expressions. To address this, we introduce a dual GAN-based head to guide the learning of the latent motion embedding, enhancing the model’s attention to fine-grained facial expressions.

Following Burkov et al. (2020); Wang et al. (2022; 2023), we employ a convolutional feature extractor network to encode the reference image into an appearance latent embedding f_{app} . Together with our motion latent code f_{mot} , these embeddings modulate a StyleGAN generator Karras et al. (2020) (i.e., the GAN-head decoder) to generate an RGB image, co-trained with our diffusion-based motion control. Its training losses, collectively denoted as L_{gan} , are formulated in image space, including a weighted L_1 reconstruction loss, adversarial loss, feature matching loss Burkov et al. (2020), and VGG perceptual losses Simonyan & Zisserman (2014); Cao et al. (2018). Focused on structural variations more than pixel-wise differences, these image-level losses guide the latent space learning with detailed and local motion modes. Furthermore, since the GAN head contains much fewer trainable parameters than the diffusion backbone, it converges faster, bootstrapping the motion encoder and aiding the learning of motion attention layers under a well-distributed motion latent embedding.

Reference Feature Masking. In line with our strategies for identity disentanglement in the motion control branch, we also aim to mitigate motion leakage from the appearance reference network. When I_R and I_D exhibit similar expressions, even just partially, the backbone network is likely to utilize the high-dimensional multi-scale appearance features as a “shortcut” for motion reference, bypassing the intended reliance on our compact 1D latent motion descriptor. While such motion leakage does not impede training data fitting during self-driven training, it hampers the learning of effective and expressive motion control (Figure 4(b)).

Inspired by Masked Image Modeling He et al. (2022), we introduce reference feature masking to mitigate motion leakage in appearance features. Specifically, we apply 30% uniform random masking to the appearance feature maps from the reference net \mathcal{R} . The masked feature maps are flattened and used as reference keys and values for the self-attention layers within the UNet backbone. This balances the strength between appearance and motion signals, ensuring that subtle driving expressions are effectively transferred without being overshadowed by the reference expressions.



397 Figure 5: Qualitative comparisons. Among all the methods, X-NeMo achieves the most accurate
398 transfer of intricate expressions and emotional subtleties while demonstrating the highest identity
399 resemblance, regardless of the characteristic differences between the reference and driving identities.
400

401 4 EXPERIMENT

402 4.1 IMPLEMENTATION DETAILS

403 We train our model on a combination of talking head datasets (HDTF Zhang et al. (2021), VFHQ Xie
404 et al. (2022)) and facial expression dataset (NerSemble Kirschstein et al. (2023)), uniformly pro-
405 cessed at 25 fps and cropped to a 512×512 resolution. The training is conducted on 8 Nvidia
406 A100 GPUs using the AdamW optimizer Yao et al. (2021) with a learning rate of $1e - 5$. We use
407 a batch size of 64 for appearance and motion control training, and a batch size of 16 for the tempo-
408 ral module using 24-frame video sequences. During inference, we implement the prompt traveling
409 technique Tseng et al. (2022) to enhance temporal smoothness in long video generation.
410
411

412 For evaluation, we compile a benchmark of 100 in-the-wild reference portraits DeviantArt (2024);
413 Midjourney (2024); Pexels (2024), representing a broad spectrum of facial structures, appearances
414 and styles. Additionally we collect 100 test videos from DFEW Jiang et al. (2020) featuring emo-
415 tionally expressive clips, alongside 200 licensed videos showcasing a diverse range of emotions,
416 head poses, and facial expressions. Please also refer to our supplementary video for more results.
417

418 4.2 EVALUATIONS AND COMPARISONS

419 In our evaluation, we compare our method against state-of-the-art video-driven portrait anima-
420 tion baselines, including X-Portrait Xie et al. (2024), AniPortrait Wei et al. (2024), Follow-your-Emoji
421 (FYE) Ma et al. (2024), and Echomimic Chen et al. (2024b). We also assess recent non-diffusion-
422 based methods, including PD-FGC Wang et al. (2023) that employs latent motion representation, and
423 LivePortrait Guo et al. (2024a) which uses implicit neural landmarks. EmoPortraits Drobyshev et al.
424 (2024), a GAN-based expressive portrait animation method, is excluded from our comparisons due
425 to the lack of inference code. For fair comparisons, we finetune AniPortrait, X-Portrait, and PD-FGC
426 using our dataset, while utilizing the released pretrained models for the remaining methods, given
427 the unavailability of their training code. We assess performance in both self and cross reenactments,
428 with all metrics computed at a resolution of 256×256 (the resolution at which PD-FGC was trained).
429

430 **Self Reenactment.** For each test video, we utilize the first frame as the reference image, generating
431 the entire sequence with subsequent frames acting as both the driving image and the ground truth
target. We evaluate the performance by computing the L1, structural (SSIM), and perceptual (LPIPS)

Table 1: Quantitative comparison. Our method achieves superior numerical results than all the baselines in both self-driven and cross-driven reenactments.

Method	Self-Reenactment			Cross-Reenactment			
	L1↓	SSIM↑	LPIPS↓	ID-SIM↑	AED/APD↓	EMO-SIM↑	FVD ↓
PD-FGC	0.085	0.728	0.291	0.604	0.045/3.95	0.49	441.8
LivePortrait	0.074	0.770	0.236	0.702	0.055/6.61	0.48	279.2
X-Portrait	0.063	0.793	0.209	0.695	0.041/4.07	0.52	237.3
FYE	0.075	0.741	0.249	0.725	0.062/4.49	0.41	360.9
AniPortrait	0.057	0.812	0.198	0.713	0.043/4.14	0.46	290.5
Ours	0.055	0.826	0.168	0.787	0.039/3.42	0.65	152.8

image losses to assess both image quality and motion accuracy. Our method, X-NeMo, consistently outperforms all baseline methods, as shown in our numerical comparisons (Table 1).

Cross Reenactment. Our method empowers the creation of captivating and expressive animations across diverse portraits even driven by in-the-wild videos with distinct identity features (Figure 1, 3, 4, 5). Our qualitative comparisons (Figure 5) demonstrate that X-NeMo surpasses all the baselines by a significant margin in identity similarity, expression accuracy and perceptual quality. GAN-based baselines suffer from blurriness and distortions under large head motions and when applied to out-of-domain portraits. For both exaggerated (e.g., cheek puffing, sticking out the tongue) and subtle facial expressions (e.g., biting the lip), all other methods struggle to faithfully capture and transfer these facial motion details. Additionally, our method excels in preserving identity resemblance, regardless of the structural difference between the reference and driving faces, while severe identity drift occurs in other diffusion-based baselines relying on spatially aligned control signals.

For quantitative assessment, given the absence of image ground truth, we employ three metrics to evaluate identity similarity, expression/head pose accuracy, and emotion consistency respectively. Specifically, we utilize the ArcFace score Deng et al. (2019) to measure the cosine similarity of identity features (ID-SIM). Motion accuracy is calculated as the average L_1 difference between extracted facial blendshapes (AED) and head poses (APD) of the driving and generated images using MediaPipe Lugaresi et al. (2019). However, since blendshapes provide only a coarse motion estimation, we further employ a pretrained emotion encoder, EmoNet Toisoul et al. (2021), to assess emotion accuracy. Specifically, we calculate the mean value of concordance correlation coefficients and Pearson correlation coefficients for both valence and arousal to measure the emotion similarity (EMO-SIM). The emotion score reflect model’s performance in fine-grained expression control, as emotion recognition is highly sensitive to micro-expressions. Our method numerically surpasses all competitors, demonstrating the superior capabilities afforded by our novel motion control design (Table 1).

Applications. Our latent motion descriptor acts as a unified representation for both motion comprehension and generation, supporting tasks beyond portrait animation, including (emotion-conditioned) portrait video outpainting and latent motion interpolation. With our expressive, identity-agnostic motion embedding, we are able to generate long-range expressive videos while consistently preserving the identity across diverse portraits. For more details and visual results, please refer to our supplemental paper (Section. E) and accompanying video.

4.3 ABLATION STUDIES

We ablate individual design choices by removing them from our full training pipeline. We validate the function of dual-head supervision in motion expressiveness by removing the GAN decoder from co-training (“w/o GAN head”). Even with extended training, the motion encoder E_{mot} struggles with detailed motions in the absence of image-level loss guidance (Figure 4(a)), as reflected by a substantial reduction in both expression and emotion metrics (Table 2). We further validate the importance of **joint** training by pretraining E_{mot} with GAN losses and then

Table 2: Quantitative ablation.

Method	ID-SIM↑	AED/APD↓	EMO-SIM↑
w/o GAN head	0.789	0.045/4.64	0.43
w/o joint training	0.782	0.040/3.49	0.52
w/o RFM	0.791	0.039/3.41	0.62
w/o augmentation	0.724	0.042/3.63	0.50
w/o cross-attn	0.697	0.040/3.55	0.48
Ours	0.787	0.039/3.42	0.65

486 freezing it while training the rest of the model solely with the diffusion loss (“w/o joint training”).
 487 Both Table 2 and the supplemental video demonstrate that joint training elicits stronger motion
 488 representation from the encoder, leveraging the diffusion model’s superior generative capacity over
 489 the standalone GAN decoder. Additionally, we assess the role of reference feature masking (“w/o
 490 RFM”) in enhancing motion accuracy. Without it, the network shows a stronger bias to the reference
 491 expressions at certain local regions(Figure 4(b)), yielding a lower emotion score (Table 2).

492 We assess the efficacy of augmentation and cross-attention control in motion-identity disentanglement.
 493 When training without augmentations (“w/o augmentation”), the generations often exhibit
 494 noticeable identity leakage from the driving subject in both appearance and face structure (Figure
 495 3(b)), as confirmed by the drop in identity similarity score (Table 2). We also compare our
 496 method to a baseline where the motion latent is transformed into a 2D control map via an upsampling
 497 decoder and applied to the UNet using a ControlNet (“w/o cross-attn”). While effective for
 498 coarse motion control, its reliance on spatially-aligned additive controls lead to reduced identity
 499 resemblance (Figure 4(a)), underscoring the necessity of our structure-agnostic motion control design.

500 We leverage classifier-free guidance
 501 (CFG) Ho & Salimans (2022) to steer
 502 the inference towards more expressive
 503 motion transfer. While straightforward
 504 for the conditional generation, we find the
 505 optimal practice by using fully masked
 506 appearance features and the motion latent
 507 f_{ref_mot} extracted from reference image
 508 I_R as the negative prompts. As illustrated
 509 in Figure 6, this CFG configuration
 510 enables the network to better distinguish
 511 between conditional appearance and
 512 motion features, facilitating more accurate and semantic motion transfer. Our CFG is formulated as

$$\tilde{\epsilon}_\theta(z_t, c_{ref}, f_{mot}) = (1 + w)\epsilon_\theta(z_t, c_{ref}, f_{mot}) - w\epsilon_\theta(z_t, \emptyset, f_{ref_mot}), \quad (2)$$

514 where $w = 3.5$ is the CFG scale and $\tilde{\epsilon}_\theta$ is the final composed noise estimate.

516 **5 DISCUSSION AND CONCLUSION**

517 We present X-NeMo, a novel diffusion-based portrait animation framework that effectively disentan-
 518 gles motion and identity, achieving substantial improvements in generating expressive, identity-
 519 preserved animations from diverse portraits. At its core, we introduce self-supervised learning
 520 framework that integrates latent motion representations with structure-agnostic motion control
 521 through cross-attentions, enhanced by carefully-designed training and inference strategies. We
 522 demonstrate high-quality animation results on a wide range of portraits and expressive driving
 523 videos, validating the efficacy of our approach. We believe our method offers valuable insights
 524 into the field and opens avenues for numerous downstream tasks. Code and model will be available
 525 for research.

526 **Limitations and Future Work.** Our
 527 method is trained solely on real human
 528 talking and expression videos. Con-
 529 sequently, out-of-domain portraits with
 530 non-human appearances, such as 3D cartoon
 531 characters, may exhibit artifacts like
 532 blurred eyes. Additionally, it might struggle
 533 with exaggerated expressions absent from the training data (see Figure 7). However, our scalable
 534 framework, free from reliance on pre-trained motion detectors, enables generalization to various
 535 styles and motions with more training data. Our motion control represents a general scheme, with
 536 which we aim to integrate into video diffusion backbones Yang et al. (2024b); Zheng et al. (2024)
 537 in the future, for smoother and more dynamic results.

538 **Ethics Statement.** Our work aims to improve portrait animation from a technical perspective and
 539 is not intended for malicious use. However, we recognize the potential for misuse like generating
 fake videos. Therefore, synthesized images and videos should clearly indicate their artificial nature.



Figure 6: Ablation on different CFG configurations.



Figure 7: Failure cases.

REFERENCES

- 540
541
542 Stability AI. Stable diffusion v1.5 model card. [https://huggingface.co/runwayml/stable-diffusion-](https://huggingface.co/runwayml/stable-diffusion-v1-5)
543 [v1-5](https://huggingface.co/runwayml/stable-diffusion-v1-5), 2022.
- 544 Andreas Blattmann, Tim Dockhorn, Sumith Kulal, Daniel Mendelevitch, Maciej Kilian, Dominik
545 Lorenz, Yam Levi, Zion English, Vikram Voleti, Adam Letts, et al. Stable video diffusion: Scaling
546 latent video diffusion models to large datasets. *arXiv preprint arXiv:2311.15127*, 2023.
- 547 Adrian Bulat and Georgios Tzimiropoulos. How far are we from solving the 2d & 3d face alignment
548 problem?(and a dataset of 230,000 3d facial landmarks). In *Proceedings of the IEEE international*
549 *conference on computer vision*, pp. 1021–1030, 2017.
- 550 Egor Burkov, Igor Pasechnik, Artur Grigorev, and Victor Lempitsky. Neural head reenactment with
551 latent pose descriptors. In *CVPR*, 2020.
- 552 Mingdeng Cao, Xintao Wang, Zhongang Qi, Ying Shan, Xiaohu Qie, and Yinqiang Zheng. Mas-
553 actrl: Tuning-free mutual self-attention control for consistent image synthesis and editing. *arXiv*
554 *preprint arXiv:2304.08465*, 2023.
- 555 Qiong Cao, Li Shen, Weidi Xie, Omkar M. Parkhi, and Andrew Zisserman. VGGFace2: A dataset
556 for recognising faces across pose and age. In *International Conference on Automatic Face and*
557 *Gesture Recognition*, 2018.
- 558 Di Chang, Yichun Shi, Quankai Gao, Hongyi Xu, Jessica Fu, Guoxian Song, Qing Yan, Yizhe Zhu,
559 Xiao Yang, and Mohammad Soleymani. Magicpose: Realistic human poses and facial expressions
560 retargeting with identity-aware diffusion. In *ICML*, 2024.
- 561 Ken Chen, Sachith Seneviratne, Wei Wang, Dongting Hu, Sanjay Saha, Md Tarek Hasan, Sanka
562 Rasnayaka, Tamasha Malepathirana, Mingming Gong, and Saman Halgamuge. Anifacediff:
563 High-fidelity face reenactment via facial parametric conditioned diffusion models. *arXiv preprint*
564 *arXiv:2406.13272*, 2024a.
- 565 Zhiyuan Chen, Jiajiong Cao, Zhiquan Chen, Yuming Li, and Chenguang Ma. Echomimic: Life-
566 like audio-driven portrait animations through editable landmark conditions. *arXiv preprint*
567 *arXiv:2407.08136*, 2024b.
- 568 Jiankang Deng, Jia Guo, Niannan Xue, and Stefanos Zafeiriou. Arcface: Additive angular margin
569 loss for deep face recognition. In *CVPR*, pp. 4690–4699, 2019.
- 570 DeviantArt. deviantart. <https://www.deviantart.com>, 2024.
- 571 Michail Christos Doukas, Stefanos Zafeiriou, and Viktoriia Sharmanska. Headgan: One-shot neural
572 head synthesis and editing. In *ICCV*, 2021.
- 573 Nikita Drobyshev, Jenya Chelishev, Taras Khakhulin, Aleksei Ivakhnenko, Victor Lempitsky, and
574 Egor Zakharov. Megaportraits: One-shot megapixel neural head avatars. In *ACM MM*, 2022.
- 575 Nikita Drobyshev, Antoni Bigata Casademunt, Konstantinos Vougioukas, Zoe Landgraf, Stavros
576 Petridis, and Maja Pantic. Emoportraits: Emotion-enhanced multimodal one-shot head avatars.
577 In *CVPR*, 2024.
- 578 Patrick Esser, Robin Rombach, and Bjorn Ommer. Taming transformers for high-resolution image
579 synthesis. In *Proceedings of the IEEE/CVF conference on computer vision and pattern recogni-*
580 *tion*, pp. 12873–12883, 2021.
- 581 Yue Gao, Yuan Zhou, Jinglu Wang, Xiao Li, Xiang Ming, and Yan Lu. High-fidelity and freely
582 controllable talking head video generation. In *CVPR*, 2023.
- 583 Ian Goodfellow, Jean Pouget-Abadie, Mehdi Mirza, Bing Xu, David Warde-Farley, Sherjil Ozair,
584 Aaron Courville, and Yoshua Bengio. Generative adversarial nets. In *NeurIPS*, 2014.
- 585 Jianzhu Guo, Dingyun Zhang, Xiaoqiang Liu, Zhizhou Zhong, Yuan Zhang, Pengfei Wan, and
586 Di Zhang. Liveportrait: Efficient portrait animation with stitching and retargeting control. *arXiv*
587 *preprint arXiv:2407.03168*, 2024a.

- 594 Yuwei Guo, Ceyuan Yang, Anyi Rao, Yaohui Wang, Yu Qiao, Dahua Lin, and Bo Dai. Animatediff:
595 Animate your personalized text-to-image diffusion models without specific tuning. *arXiv preprint*
596 *arXiv:2307.04725*, 2023.
- 597 Yuwei Guo, Ceyuan Yang, Anyi Rao, Zhengyang Liang, Yaohui Wang, Yu Qiao, Maneesh
598 Agrawala, Dahua Lin, and Bo Dai. Animatediff: Animate your personalized text-to-image diffu-
599 sion models without specific tuning. In *ICLR*, 2024b.
- 600 Yue Han, Jiangning Zhang, Junwei Zhu, Xiangtai Li, Yanhao Ge, Wei Li, Chengjie Wang, Yong
601 Liu, Xiaoming Liu, and Ying Tai. A generalist face via learning unified facial representation.
602 *arXiv preprint arXiv:2401.00551*, 2023.
- 603 Kaiming He, Xinlei Chen, Saining Xie, Yanghao Li, Piotr Dollár, and Ross Girshick. Masked
604 autoencoders are scalable vision learners. In *CVPR*, pp. 16000–16009, 2022.
- 605 Jonathan Ho and Tim Salimans. Classifier-free diffusion guidance. *arXiv preprint*
606 *arXiv:2207.12598*, 2022.
- 607 Jonathan Ho, Ajay Jain, and Pieter Abbeel. Denoising diffusion probabilistic models. *NeurIPS*, 33:
608 6840–6851, 2020.
- 609 Li Hu, Xin Gao, Peng Zhang, Ke Sun, Bang Zhang, and Liefeng Bo. Animate anyone:
610 Consistent and controllable image-to-video synthesis for character animation. *arXiv preprint*
611 *arXiv:2311.17117*, 2023.
- 612 Xingxun Jiang, Yuan Zong, Wenming Zheng, Chuangao Tang, Wanchuang Xia, Cheng Lu, and
613 Jiateng Liu. Dfew: A large-scale database for recognizing dynamic facial expressions in the wild.
614 In *Proceedings of the 28th ACM international conference on multimedia*, pp. 2881–2889, 2020.
- 615 Tero Karras, Samuli Laine, and Timo Aila. A style-based generator architecture for generative
616 adversarial networks. In *CVPR*, 2019.
- 617 Tero Karras, Samuli Laine, Miika Aittala, Janne Hellsten, Jaakko Lehtinen, and Timo Aila. Analyz-
618 ing and improving the image quality of StyleGAN. In *CVPR*, 2020.
- 619 Apoorv Khandelwal, Luca Weihs, Roozbeh Mottaghi, and Aniruddha Kembhavi. Simple but effec-
620 tive: Clip embeddings for embodied ai. In *Proceedings of the IEEE/CVF Conference on Computer*
621 *Vision and Pattern Recognition*, pp. 14829–14838, 2022.
- 622 Tobias Kirschstein, Shenhan Qian, Simon Giebenhain, Tim Walter, and Matthias Nießner. Nersem-
623 ble: Multi-view radiance field reconstruction of human heads. *ACM Transactions on Graphics*,
624 2023.
- 625 Borong Liang, Yan Pan, Zhizhi Guo, Hang Zhou, Zhibin Hong, Xiaoguang Han, Junyu Han, Jingtuo
626 Liu, Errui Ding, and Jingdong Wang. Expressive talking head generation with granular audio-
627 visual control. In *CVPR*, 2022.
- 628 Renshuai Liu, Bowen Ma, Wei Zhang, Zhipeng Hu, Changjie Fan, Tangjie Lv, Yu Ding, and Xuan
629 Cheng. Towards a simultaneous and granular identity-expression control in personalized face
630 generation. In *CVPR*, 2024.
- 631 Camillo Lugaresi, Jiuqiang Tang, Hadon Nash, Chris McClanahan, Esha Uboweja, Michael Hays,
632 Fan Zhang, Chuo-Ling Chang, Ming Guang Yong, Juhyun Lee, et al. Mediapipe: A framework
633 for building perception pipelines. *arXiv preprint arXiv:1906.08172*, 2019.
- 634 Yue Ma, Hongyu Liu, Hongfa Wang, Heng Pan, Yingqing He, Junkun Yuan, Ailing Zeng, Chengfei
635 Cai, Heung-Yeung Shum, Wei Liu, et al. Follow-your-emoji: Fine-controllable and expressive
636 freestyle portrait animation. *arXiv preprint arXiv:2406.01900*, 2024.
- 637 Arun Mallya, Ting-Chun Wang, and Ming-Yu Liu. Implicit warping for animation with image sets.
638 *NeurIPS*, 2022.
- 639 Midjourney. midjourney. <https://www.midjourney.com>, 2024.

- 648 Youxin Pang, Yong Zhang, Weize Quan, Yanbo Fan, Xiaodong Cun, Ying Shan, and Dong-ming
649 Yan. Dpe: Disentanglement of pose and expression for general video portrait editing. In *CVPR*,
650 2023.
- 651 Reni Paskaleva, Mykyta Holubakha, Andela Ilic, Saman Motamed, Luc Van Gool, and Danda
652 Paudel. A unified and interpretable emotion representation and expression generation. In *CVPR*,
653 2024.
- 654 Pexels. pexels. <https://www.pexels.com/>, 2024.
- 655 Yurui Ren, Ge Li, Yuanqi Chen, Thomas H Li, and Shan Liu. Pirenderer: Controllable portrait
656 image generation via semantic neural rendering. In *ICCV*, 2021.
- 657 Robin Rombach, Andreas Blattmann, Dominik Lorenz, Patrick Esser, and Björn Ommer. High-
658 resolution image synthesis with latent diffusion models. In *CVPR*, pp. 10684–10695, 2022.
- 659 Nataniel Ruiz, Yuanzhen Li, Varun Jampani, Yael Pritch, Michael Rubinstein, and Kfir Aberman.
660 Dreambooth: Fine tuning text-to-image diffusion models for subject-driven generation. In *Pro-
661 ceedings of the IEEE/CVF conference on computer vision and pattern recognition*, pp. 22500–
662 22510, 2023.
- 663 Chitwan Saharia, William Chan, Saurabh Saxena, Lala Li, Jay Whang, Emily L Denton, Kamyar
664 Ghasemipour, Raphael Gontijo Lopes, Burcu Karagol Ayan, Tim Salimans, et al. Photorealistic
665 text-to-image diffusion models with deep language understanding. *NeurIPS*, 35:36479–36494,
666 2022.
- 667 Aliaksandr Siarohin, Stéphane Lathuilière, Sergey Tulyakov, Elisa Ricci, and Nicu Sebe. Animating
668 arbitrary objects via deep motion transfer. In *CVPR*, 2019a.
- 669 Aliaksandr Siarohin, Stéphane Lathuilière, Sergey Tulyakov, Elisa Ricci, and Nicu Sebe. First order
670 motion model for image animation. *NeurIPS*, 2019b.
- 671 Karen Simonyan and Andrew Zisserman. Very deep convolutional networks for large-scale image
672 recognition. *arXiv preprint arXiv:1409.1556*, 2014.
- 673 Jiaming Song, Chenlin Meng, and Stefano Ermon. Denoising diffusion implicit models. *arXiv
674 preprint arXiv:2010.02502*, 2020a.
- 675 Yang Song, Jascha Sohl-Dickstein, Diederik P Kingma, Abhishek Kumar, Stefano Ermon, and Ben
676 Poole. Score-based generative modeling through stochastic differential equations. *arXiv preprint
677 arXiv:2011.13456*, 2020b.
- 678 Linrui Tian, Qi Wang, Bang Zhang, and Liefeng Bo. Emo: Emote portrait alive-generating expres-
679 sive portrait videos with audio2video diffusion model under weak conditions. In *ECCV*, 2024.
- 680 Naftali Tishby, Fernando C Pereira, and William Bialek. The information bottleneck method. *arXiv
681 preprint physics/0004057*, 2000.
- 682 Antoine Toisoul, Jean Kossaiifi, Adrian Bulat, Georgios Tzimiropoulos, and Maja Pantic. Es-
683 timation of continuous valence and arousal levels from faces in naturalistic conditions.
684 *Nature Machine Intelligence*, 2021. URL [https://www.nature.com/articles/
685 s42256-020-00280-0](https://www.nature.com/articles/s42256-020-00280-0).
- 686 Jonathan Tseng, Rodrigo Castellon, and C. Karen Liu. Edge: Editable dance generation from music,
687 2022.
- 688 Tuomas Varanka, Huai-Qian Khor, Yante Li, Mengting Wei, Hanwei Kung, Nicu Sebe, and Guoying
689 Zhao. Towards localized fine-grained control for facial expression generation. *arXiv preprint
690 arXiv:2407.20175*, 2024.
- 691 Cong Wang, Kuan Tian, Jun Zhang, Yonghang Guan, Feng Luo, Fei Shen, Zhiwei Jiang, Qing Gu,
692 Xiao Han, and Wei Yang. V-express: Conditional dropout for progressive training of portrait
693 video generation. *arXiv preprint arXiv:2406.02511*, 2024.

- 702 Duomin Wang, Yu Deng, Zixin Yin, Heung-Yeung Shum, and Baoyuan Wang. Progressive dis-
703 entangled representation learning for fine-grained controllable talking head synthesis. In *CVPR*,
704 2023.
- 705 Kaisiyuan Wang, Qianyi Wu, Linsen Song, Zhuoqian Yang, Wayne Wu, Chen Qian, Ran He,
706 Yu Qiao, and Chen Change Loy. Mead: A large-scale audio-visual dataset for emotional talking-
707 face generation. In *European Conference on Computer Vision*, pp. 700–717. Springer, 2020.
- 708 Ting-Chun Wang, Arun Mallya, and Ming-Yu Liu. One-shot free-view neural talking-head synthesis
709 for video conferencing. In *CVPR*, 2021.
- 710 Yaohui Wang, Di Yang, Francois Bremond, and Antitza Dantcheva. Latent image animator: Learn-
711 ing to animate images via latent space navigation. *ICLR*, 2022.
- 712 Huawei Wei, Zejun Yang, and Zhisheng Wang. Aniportrait: Audio-driven synthesis of photorealistic
713 portrait animation. *arXiv preprint arXiv:2403.17694*, 2024.
- 714 Liangbin Xie, Xintao Wang, Honglun Zhang, Chao Dong, and Ying Shan. Vfhq: A high-quality
715 dataset and benchmark for video face super-resolution. In *The IEEE Conference on Computer*
716 *Vision and Pattern Recognition Workshops (CVPRW)*, 2022.
- 717 You Xie, Hongyi Xu, Guoxian Song, Chao Wang, Yichun Shi, and Linjie Luo. X-portrait: Expres-
718 sive portrait animation with hierarchical motion attention. In *SIGGRAPH*, 2024.
- 719 Chao Xu, Yang Liu, Jiazheng Xing, Weida Wang, Mingze Sun, Jun Dan, Tianxin Huang, Siyuan Li,
720 Zhi-Qi Cheng, Ying Tai, et al. Facechain-imagineid: Freely crafting high-fidelity diverse talking
721 faces from disentangled audio. In *CVPR*, 2024a.
- 722 Mingwang Xu, Hui Li, Qingkun Su, Hanlin Shang, Liwei Zhang, Ce Liu, Jingdong Wang, Luc
723 Van Gool, Yao Yao, and Siyu Zhu. Hallo: Hierarchical audio-driven visual synthesis for portrait
724 image animation. *arXiv preprint arXiv:2406.08801*, 2024b.
- 725 Sicheng Xu, Guojun Chen, Yu-Xiao Guo, Jiaolong Yang, Chong Li, Zhenyu Zang, Yizhong Zhang,
726 Xin Tong, and Baining Guo. Vasa-1: Lifelike audio-driven talking faces generated in real time.
727 *arXiv preprint arXiv:2404.10667*, 2024c.
- 728 Zhongcong Xu, Jianfeng Zhang, Jun Hao Liew, Hanshu Yan, Jia-Wei Liu, Chenxu Zhang, Jiashi
729 Feng, and Mike Zheng Shou. Magicanimate: Temporally consistent human image animation
730 using diffusion model. In *CVPR*, 2024d.
- 731 Shurong Yang, Huadong Li, Juhao Wu, Minhao Jing, Linze Li, Renhe Ji, Jiajun Liang, and Haoqiang
732 Fan. Megactor: Harness the power of raw video for vivid portrait animation. *arXiv preprint*
733 *arXiv:2405.20851*, 2024a.
- 734 Zhuoyi Yang, Jiayan Teng, Wendi Zheng, Ming Ding, Shiyu Huang, Jiazheng Xu, Yuanming Yang,
735 Wenyi Hong, Xiaohan Zhang, Guanyu Feng, et al. Cogvideox: Text-to-video diffusion models
736 with an expert transformer. *arXiv preprint arXiv:2408.06072*, 2024b.
- 737 Zhewei Yao, Amir Gholami, Sheng Shen, Mustafa Mustafa, Kurt Keutzer, and Michael Mahoney.
738 Adahessian: An adaptive second order optimizer for machine learning. In *proceedings of the*
739 *AAAI conference on artificial intelligence*, volume 35, pp. 10665–10673, 2021.
- 740 Fei Yin, Yong Zhang, Xiaodong Cun, Mingdeng Cao, Yanbo Fan, Xuan Wang, Qingyan Bai,
741 Baoyuan Wu, Jue Wang, and Yujiu Yang. Styleheat: One-shot high-resolution editable talking
742 face generation via pre-trained stylegan. In *ECCV*, 2022.
- 743 Jianrong Zhang, Yangsong Zhang, Xiaodong Cun, Shaoli Huang, Yong Zhang, Hongwei Zhao,
744 Hongtao Lu, and Xi Shen. T2m-gpt: Generating human motion from textual descriptions with
745 discrete representations. In *CVPR*, 2023a.
- 746 Lvmin Zhang, Anyi Rao, and Maneesh Agrawala. Adding conditional control to text-to-image
747 diffusion models. In *ICCV*, pp. 3836–3847, 2023b.

Zhimeng Zhang, Lincheng Li, Yu Ding, and Changjie Fan. Flow-guided one-shot talking face generation with a high-resolution audio-visual dataset. In *CVPR*, pp. 3661–3670, 2021.

Jian Zhao and Hui Zhang. Thin-plate spline motion model for image animation. In *CVPR*, 2022.

Zangwei Zheng, Xiangyu Peng, Tianji Yang, Chenhui Shen, Shenggui Li, Hongxin Liu, Yukun Zhou, Tianyi Li, and Yang You. Open-sora: Democratizing efficient video production for all, March 2024. URL <https://github.com/hpcaitech/Open-Sora>.

Hang Zhou, Yasheng Sun, Wayne Wu, Chen Change Loy, Xiaogang Wang, and Ziwei Liu. Pose-controllable talking face generation by implicitly modularized audio-visual representation. In *CVPR*, 2021.

A TRAINING AND INFERENCE DETAILS

GAN Head Training Losses. Following Burkov et al. (2020), we train our dual GAN decoder in a self-supervised manner to reconstruct I_D using a combination of losses. Specifically, a L_1 reconstruction loss is employed to minimize pixel-wise L_1 distance:

$$\mathcal{L}_{recon} = \|I_D - I_{R \rightarrow D}\|_1 \quad (3)$$

Additionally, two perceptual losses, L_{VGG} and $L_{VGGFace}$, are applied based on L_1 matching of ConvNet activations from a VGG-19 model Simonyan & Zisserman (2014) pretrained for ImageNet classification and a VGGFace model Cao et al. (2018) trained for face recognition:

$$\mathcal{L}_{vgg} = \sum_{i=1}^N \|VGG^i(I_D) - VGG^i(I_{R \rightarrow D})\|_1, \quad (4)$$

$$\mathcal{L}_{vggf} = \sum_{I=1}^N \|VGG_{face}^i(I_D) - VGG_{face}^i(I_{R \rightarrow D})\|_1, \quad (5)$$

where N denotes the number of feature layers in each respective pre-trained VGG model. An adversarial generative loss L_{adv} is applied using a co-trained discriminator D , while a feature matching loss L_{fm} is calculated as the L_1 distance between discriminator feature maps at different layers:

$$\mathcal{L}_{fm} = \sum_{i=1}^N \|D^i(I_D) - D^i(I_{R \rightarrow D})\|_1 \quad (6)$$

The overall learning objective for the GAN head is then formulated as:

$$\mathcal{L}_{gan} = \mathcal{L}_{adv} + \lambda_r \mathcal{L}_{recon} + \lambda_{vgg} \mathcal{L}_{vgg} + \lambda_{vggf} \mathcal{L}_{vggf} + \lambda_{fm} \mathcal{L}_{fm} \quad (7)$$

where $\lambda_r=1.0$, $\lambda_{vgg}=3e-2$, $\lambda_{vggf}=6e-3$ and $\lambda_{fm}=10.0$.

Inference Performance. During inference, we use 25 DDIM steps Song et al. (2020a) with a classifier-free guidance (CFG) scale of 3.5. For generating a 1-second video at 25 frames per second, the process takes approximately 20 seconds and requires 24 GB of memory.

Encoder Architecture. E_{mot} takes the classical feature alignment network Bulat & Tzimiropoulos (2017) as the backbone, with an additional attention layer added at both its input and output to enhance feature extraction capabilities. Finally, it outputs a 1D vector through two MLP layers. The appearance encoder for extracting f_{app} is implemented as a ResNet50.

B VIDEO-LEVEL PERFORMANCE ANALYSIS

As demonstrated in our comprehensive quantitative (Table 1) and qualitative evaluations (Figure 5 and video demos), X-NeMo consistently outperforms all baseline methods in motion expressiveness and temporal coherence. This strong video-level performance stems primarily from our robust

single-frame reenactment capability. Specifically, our motion encoder captures fine-scale facial motion within individual frames, while the temporal motion module focuses on cross-frame consistency, supported by the SVD-VAE decoder Blattmann et al. (2023) and prompt traveling Cao et al. (2023) during inference.

Unlike prior methods, which rely on pre-trained motion control signals such as explicit landmarks (AniPortrait Wei et al. (2024)) or implicit landmarks (X-Portrait Xie et al. (2024)), our approach utilizes a learnable motion representation that is optimized jointly with the diffusion generator. Pre-trained motion signals are often unstable and prone to jitter across frames, and they fail to fully capture the complex facial expressions present in diverse datasets. By jointly optimizing motion representation with the generator, X-NeMo inherently achieves better expressiveness and more effective disentanglement of motion and identity.

However, straightforward self-supervised training does not naturally disentangle identity from facial motion. As shown in Table 2, critical components like Dual Head Supervision, Cross-Attention, and Augmentations are essential for achieving effective disentanglement. Furthermore, Joint Training and RFM enhance motion extraction, capturing subtle micro-expressions (not captured by AKD but reflected in the EMO-SIM metric) and enabling vivid and expressive reenactment results.

C MORE ABLATIONS

We provide additional visual ablations on some network and training hyperparameters.

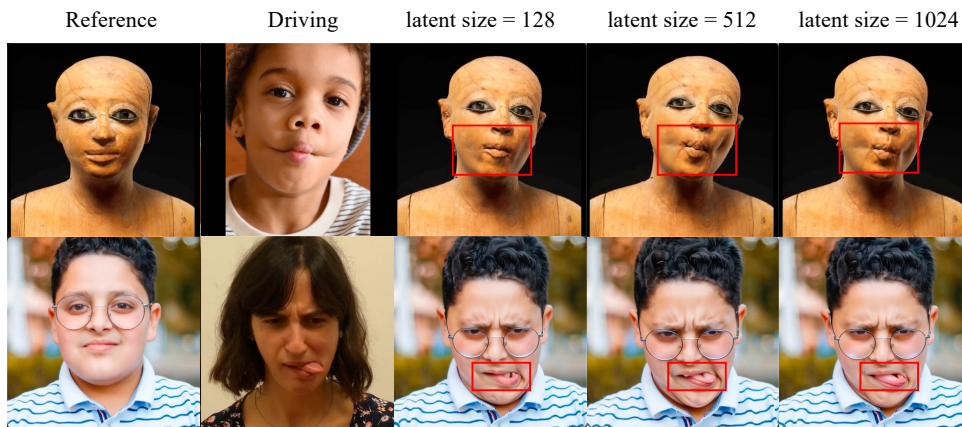
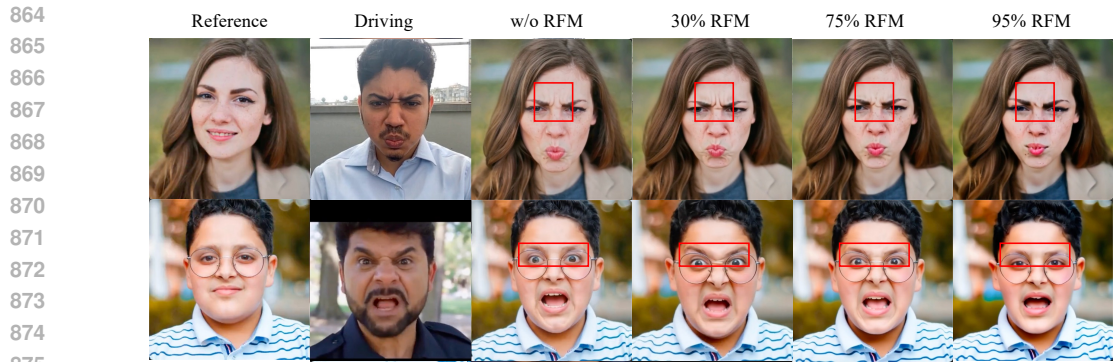


Figure 8: We ablate the effect of different sizes of latent motion embedding in capturing fine-grained intricate expressions.

Motion Latent Embedding Size. We evaluate the dimensionality of our motion latent embedding by comparing 128, 512, and 1024-dimensional latent codes for f_{mot} . In typical driving scenarios, all three configurations perform similarly in replicating facial expressions with minimal differences. However, as shown in Figure 8, reducing the embedding size to 128 diminishes the ability to capture subtle, intricate expressions, while increasing it to 1024 provides negligible improvements. Thus, we select the 512-dimensional embedding as it balances compactness with motion expressiveness.

Reference Feature Masking Ratio. We assess the effectiveness of our reference feature masking strategy across different masking ratios, ranging from 0%, 30%, 75%, to 95%. As shown in Figure 9, this strategy enhances the transfer of detailed facial expressions; however, excessively high masking ratios impede the model’s ability to capture fine motion details and maintain identity consistency. This is likely because when the reference image’s appearance is too heavily obscured during training, the motion encoder compensates by encoding appearance information, reducing the capacity of the motion embedding for expressing dynamic movements. In practice, we found that masking ratios between 20% and 50% achieve optimal results, with 30% used in our implementation.



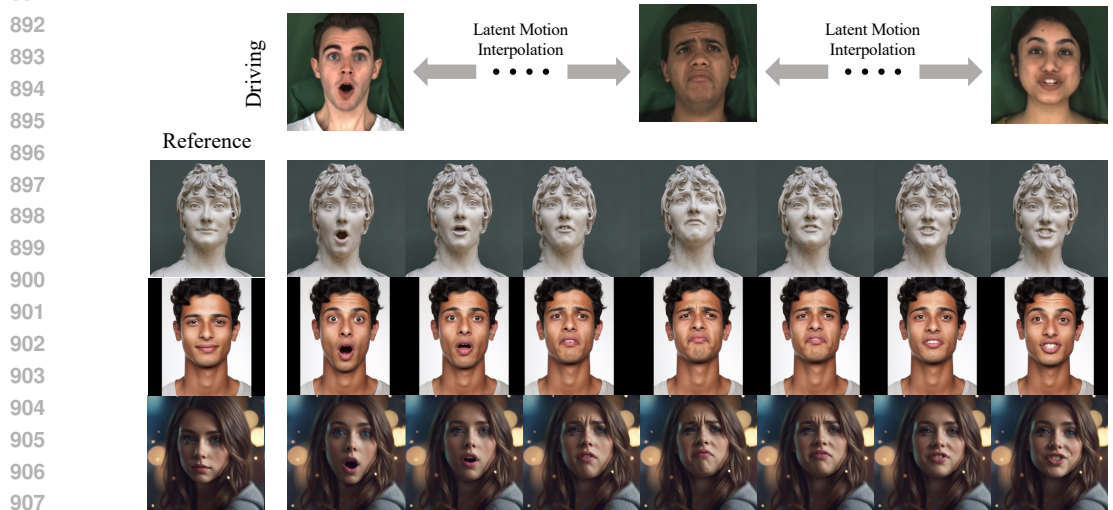
876 Figure 9: Qualitative comparison of different ratios of reference feature masking indicates that 30%
877 achieves the most accurate capture of driving facial motions.
878

880 **D MORE RESULTS**

881 Please refer to our supplemental video for more expressive demo cases.
882
883
884

885 **E APPLICATIONS**

886 Our latent motion embedding, trained *jointly* with the diffusion backbone, offers a compact, identity-
887 agnostic, yet expressive representation for a diverse range of facial motions. Beyond the primary
888 portrait animation task, we showcase its broader applications as a unified motion representation,
889 enabling seamless motion interpolation, video outpainting and conditioned generation.
890



909 Figure 10: Latent motion interpolation. We derive latent motion codes from a few driving keyframes
910 (top) and apply onto diverse portraits with linearly interpolated motion embeddings (bottom).
911

912
913 **Latent Motion Interpolation.** Owing to our smooth and identity-agnostic latent motion space, we
914 are able to extract keyframe expressions from different videos, linearly interpolate the latent embed-
915 dings and apply them across diverse portraits, as showcased in Figure. 10. This interpolation yields
916 smooth and natural expression transitions, maintaining motion coherence across different portraits
917 and appearance consistency with the reference images. These results underscore the robustness and
identity disentanglement of our motion latent embedding.

Portrait Video Outpainting and Generation. By leveraging our motion latent embedding as a unified representation for motion comprehension and generation, we showcase its application in video outpainting. Specifically, we adopt the approach from T2M-GPT Zhang et al. (2023a) to tokenize temporal latent motions by training a Vector-Quantized VAE model Esser et al. (2021) with a learnable codebook (4096 entries of 8-dimension code) that downsamples the temporal dimension by a factor of 4. This allows us to represent T frames of motion with $T/4$ discrete motion tokens, where T is the training sequence length (we use $T = 128$), facilitating the use of GPT-like frameworks for long-sequence motion generation. In Figure. 12, we train a GPT2-small network that extends preceding motions derived from a driving video with extrapolated motions. The results show natural and expressive generated sequences, thanks to the strong representation power of our latent motion embedding. Moreover, as more facial video datasets containing multimodal annotations (e.g., text and audio) become available, our method can seamlessly extend to multimodal facial video generation within a unified framework. As an example, we illustrate emotion-conditioned portrait video generation in Figure 11, trained with MEAD dataset Wang et al. (2020).

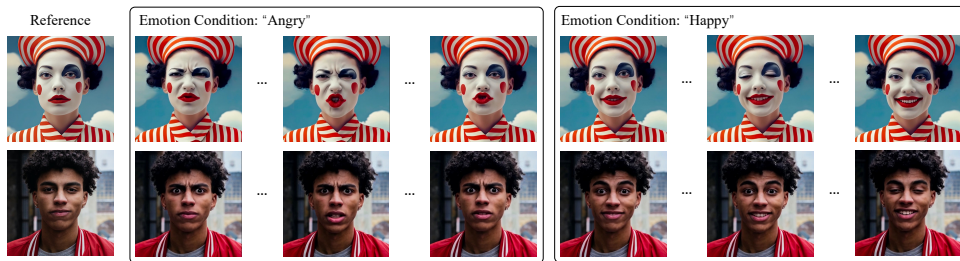


Figure 11: Emotion-conditioned portrait video generation.

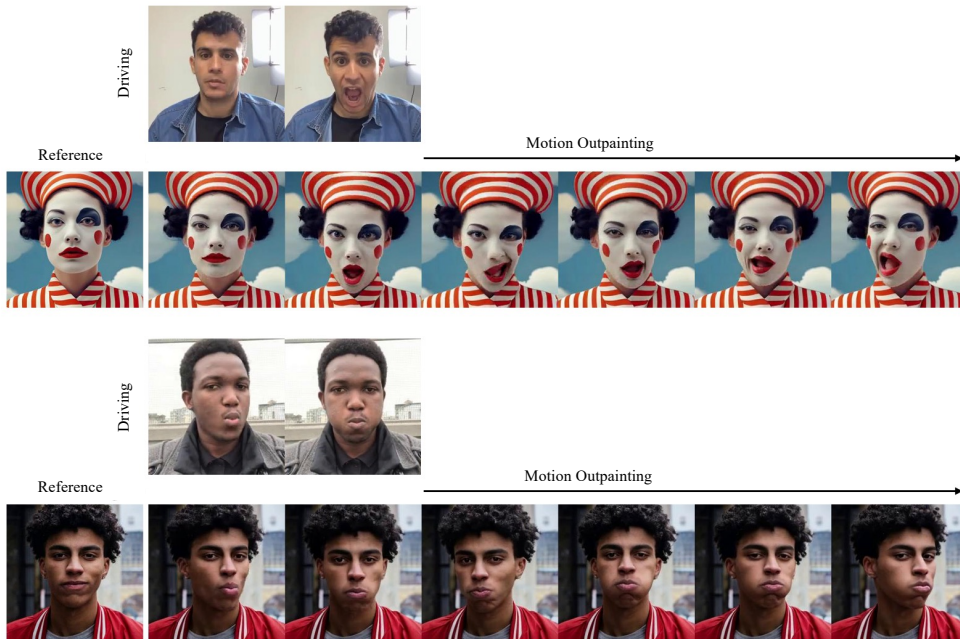


Figure 12: Portrait video outpainting. Starting from a sequence of driving motion, our model is capable of extrapolating into a long video sequence with consistent identity attributes.

972

973

974

975

976

977

978

979

980

981

982

983

984

985

986

987

988

989

990

991

992

993

994

995

996

997

998

999

1000

1001

1002

1003

1004

1005

1006

1007

1008

1009

1010

1011

1012

1013

1014

1015

1016

1017

1018

1019

1020

1021

1022

1023

1024

1025

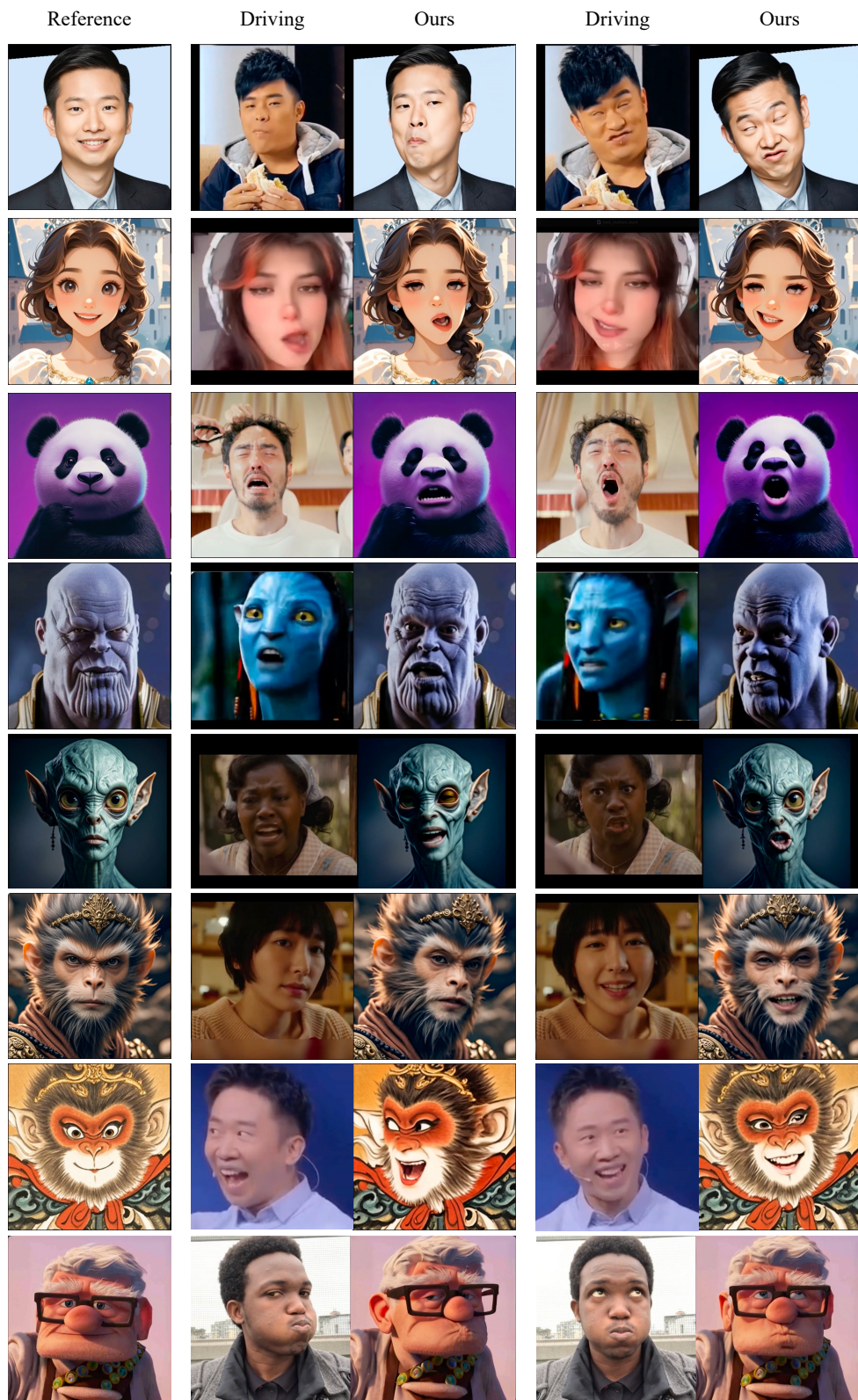


Figure 13: Our method demonstrates strong generalization capabilities, effectively handling out-of-domain exaggerated facial motions (top two rows) and non-human appearances (bottom six rows).